

Parametrizing the Reionization History with the Redshift Midpoint, Duration, and Asymmetry

HY TRAC¹

¹*McWilliams Center for Cosmology, Department of Physics, Carnegie Mellon University, Pittsburgh, PA 15213*

Submitted to ApJL

ABSTRACT

A new parametrization of the reionization history is presented to facilitate robust comparisons between different observations and with theory. The evolution of the ionization fraction with redshift can be effectively captured by specifying the midpoint, duration, and asymmetry parameters. Lagrange interpolating functions are then used to construct analytical curves which exactly fit corresponding ionization points. The shape parametrizations are excellent matches to theoretical results from radiation-hydrodynamic simulations. The comparative differences for reionization observables are: ionization fraction $|\Delta x_i| \lesssim 0.03$, 21cm brightness temperature $|\Delta T_b| \lesssim 0.7 \text{ mK}$, Thompson optical depth $|\Delta \tau| \lesssim 0.001$, and patchy kinetic Sunyaev-Zel'dovich angular power $|\Delta D_\ell| \lesssim 0.1 \mu\text{K}^2$. This accurate and flexible approach will allow parameter-space studies and self-consistent constraints on the reionization history from 21cm, CMB, and high-redshift galaxies and quasars.

Keywords: cosmology: theory – dark ages, reionization, first stars – galaxies: high-redshift – methods: analytical – numerical

1. INTRODUCTION

The reionization of hydrogen by the first stars, galaxies, and quasars is a milestone event in the first billion years. Ionizing radiation from luminous sources convert the cold and neutral gas into a warm and highly ionized medium (Loeb & Furlanetto 2013, for a review). Recent observations suggest that the epoch of reionization (EoR) was already in significant progress by redshift $z \sim 8$ and must have ended by $z \sim 6$ (Planck Collaboration et al. 2016a, and references therein). Upcoming observations will better constrain the reionization history, as well as the abundance and properties of the radiation sources.

The reionization history is quantified by the evolution of the ionization fraction $x_i(z)$. It is used in the calculation of EoR observables such as the 21cm brightness temperature (e.g. Madau et al. 1997; Furlanetto et al. 2006), Thomson optical depth, cosmic microwave background (CMB) temperature and polarization anisotropies (e.g. Bond & Efstathiou 1987; Zaldarriaga 1997), and kinetic Sunyaev-Zel'dovich (KSZ) effect (e.g. Sunyaev & Zeldovich 1970; Ostriker & Vishniac 1986). Thus, it is important to establish a standard parametrization of the reionization history to facilitate robust comparisons between different observations and with theory.

The ionization fraction is often parametrized using a tanh function with two free parameters which set the redshift midpoint and width (Lewis 2008). However, the width parameter does not clearly define the duration of the EoR and the simple functional form does not allow for possible asymmetry. Redshift-asymmetric parameterizations using polynomials, exponentials, and power-laws have recently been proposed (e.g. Douspis et al. 2015; Planck Collaboration et al. 2016a). Generalized logistic functions (Richards 1959) can have asymmetric sigmoid shapes, but the physical interpretation of some of the free parameters for reionization is not straightforward.

In this Letter, I present an accurate parametrization of the reionization history in terms of the redshift midpoint, duration, and asymmetry. Lagrange interpolating functions are used to construct analytical curves which exactly fit corresponding ionization points. The shape parametrizations are then compared against radiation-hydrodynamic simulations from the Simulations and Constructions of the Reionization of Cosmic Hydrogen (SCORCH) project (Trac et al. 2015; Doussot et al. 2017). The adopted cosmological parameters are: $\Omega_m = 0.3$, $\Omega_\Lambda = 0.7$, $\Omega_b = 0.045$, $h = 0.7$, $\sigma_8 = 0.8$, $n_s = 0.96$, $Y_{\text{He}} = 0.24$, and $T_{\text{CMB}} = 2.725 \text{ K}$.

2. METHODS

2.1. Midpoint, Duration, and Asymmetry

The reionization history is quantified by the ionized hydrogen fraction, which can be mass-weighted or volume-weighted. I will work with the mass-weighted version $x_{i,M}$ since the volume-averaged ionized hydrogen number density is given by

$$\bar{n}_{\text{HII},V} = x_{i,M} \bar{n}_{\text{H},V}. \quad (1)$$

From here on, the mass-weighted and volume-averaged subscripts will be dropped to simplify the notation. Also, let z_x denote the redshift corresponding to the ionization factor $x = 100x_i$.

In [Doussot et al. \(2017\)](#), we choose the redshift midpoint as z_{50} and present two practical choices for defining the duration Δ_z and asymmetry A_z parameters. In the first case:

$$\begin{aligned} \Delta_{z50} &\equiv z_{25} - z_{75}, \\ A_{z50} &\equiv \frac{z_{25} - z_{50}}{z_{50} - z_{75}}, \end{aligned} \quad (2)$$

the redshifts correspond to quartile ionization fractions ($x_i = 0.25, 0.50, 0.75$) and Δ_{z50} is analogous to a full width half max. In the second case:

$$\begin{aligned} \Delta_{z90} &\equiv z_{05} - z_{95}, \\ A_{z90} &\equiv \frac{z_{05} - z_{50}}{z_{50} - z_{95}}, \end{aligned} \quad (3)$$

the redshifts correspond to early and late ionization fractions ($x_i = 0.05, 0.95$) and Δ_{z90} effectively quantifies the full extent of the EoR. While other definitions (e.g. $\Delta_{z68}, \Delta_{z95}$) can be adopted, extreme choices (e.g. Δ_{z99}) are not recommended since the start and end of the EoR are difficult to determine precisely.

2.2. Lagrange Interpolating Functions

Given the midpoint, duration, and asymmetry parameters, the relevant redshifts are uniquely specified and given by

$$\begin{aligned} z_{25} &= z_{50} + \frac{\Delta_{z50} A_{z50}}{1 + A_{z50}}, \\ z_{75} &= z_{25} - \Delta_{z50}, \end{aligned} \quad (4)$$

or

$$\begin{aligned} z_{05} &= z_{50} + \frac{\Delta_{z90} A_{z90}}{1 + A_{z90}}, \\ z_{95} &= z_{05} - \Delta_{z90}. \end{aligned} \quad (5)$$

An analytical function that exactly passes through a given set of ionization points and therefore satisfies the

Table 1. The redshift midpoint, duration, and asymmetry parameters for three RadHydro simulations from the SCORCH project.

Model	z_{50}	Δ_{z50}	Δ_{z90}	A_{z50}	A_{z90}
Sim 0	7.95	1.87	4.68	1.63	2.90
Sim 1	7.91	2.27	5.45	1.59	2.69
Sim 2	7.83	2.89	6.54	1.49	2.33

chosen midpoint, duration, and asymmetry parameters can be constructed using the method of Lagrange interpolation. In practice, a straightforward interpolation of x_i in terms of z or $1+z$ can have oscillations, but the approach works better with a simple change of variables,

$$\begin{aligned} u &= \ln(1+z), \\ v &= \ln x_i. \end{aligned} \quad (6)$$

For N points, a polynomial $v(u)$ of degree $N-1$ can be constructed as

$$\begin{aligned} v(u) &= \sum_{j=1}^N p_j(u), \\ p_j(u) &= v_j \prod_{\substack{k=1 \\ k \neq j}}^N \frac{u - u_k}{u_j - u_k}. \end{aligned} \quad (7)$$

The ionization fraction $x_i(z) = \exp[v(u)]$ has the advantages of being continuous, differentiable, integratable, and invertible. At higher redshifts towards the start of the EoR, x_i asymptotically goes to zero as required. At lower redshifts after the end of reionization, a physical maximum limit of unity should be imposed in practice.

2.3. Radiation-Hydrodynamic Simulations

To test the accuracy of the analytical parametrizations, I compare them against simulation results from the SCORCH project. In [Doussot et al. \(2017\)](#), we present three reionization simulations with the same galaxy luminosity functions, but with different radiation escape fraction $f_{\text{esc}}(z)$ models. The simulations are designed to have fixed Thomson optical depth $\tau \approx 0.06$, consistent with recent CMB observations (e.g. [Planck Collaboration et al. 2016a,b](#)).

The simulations are run with the RadHydro code, which combines N-body and hydrodynamic algorithms ([Trac & Pen 2004](#)) with an adaptive raytracing algorithm ([Trac & Cen 2007](#)) to directly and simultaneously solve collisionless dark matter dynamics, collisional gas dynamics, and radiative transfer of ionizing photons.

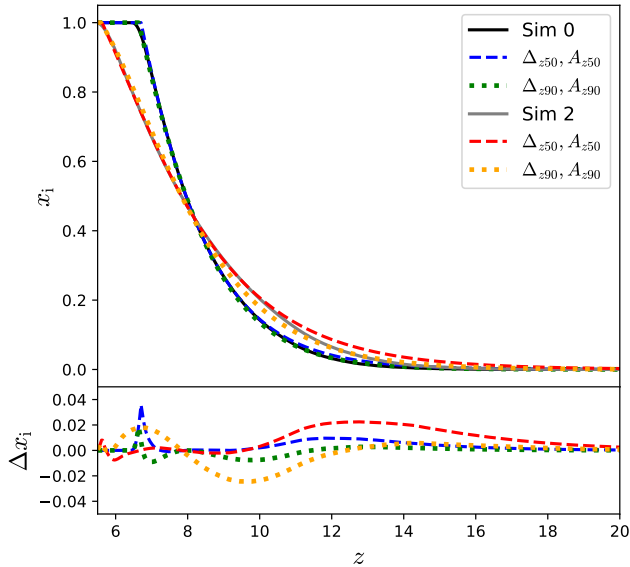


Figure 1. Top: The evolution of the mass-weighted ionization fraction with redshift. The analytical parametrizations accurately capture the redshift-asymmetric form of the simulation curves. **Bottom:** The typical differences in ionization fractions are $|\Delta x_i| \lesssim 0.02$, while the maximum differences of $|\Delta x_i| \lesssim 0.03$ are found near the start and end of the EoR, which are uncertain in the simulations.

Each RadHydro simulation has 2048^3 dark matter particles, 2048^3 gas cells, and up to 12 billion adaptive rays in a comoving box of side length $50 h^{-1}\text{Mpc}$.

Table 1 lists the midpoint, duration, and asymmetry parameters for the three SCORCH simulations. The index in the model name reflects the power-law slope in the evolution of the radiation escape fraction with $1+z$. Sim 0 has constant f_{esc} and reionization starts latest, but ends earliest out of the three models. Sim 1 has $f_{\text{esc}}(z)$ varying linearly and is an intermediate model. Sim 2 has $f_{\text{esc}}(z)$ varying quadratically and reionization starts earliest, but ends latest.

3. RESULTS

3.1. Ionization Fraction

Figure 1 shows the evolution of the ionization fraction for the redshift range $5.5 < z < 20$. Only Sim 0 and Sim 2 are shown for clarity since Sim 1 gives intermediate results. The analytical parametrizations are excellent matches to the simulation results and the typical differences are only $|\Delta x_i| \lesssim 0.02$. The maximum differences of $|\Delta x_i| \lesssim 0.03$ are found near the start and end of the EoR, which are also not accurately captured in reionization simulations and semi-analytical models.

The shape parametrizations using Δ_{z50} and A_{z50} produce more accurate results near the midpoint, while those with Δ_{z90} and A_{z90} produce smaller differences

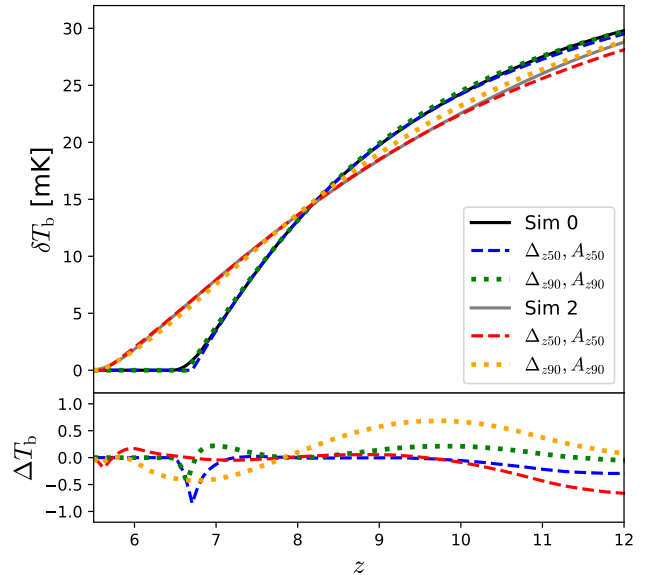


Figure 2. Top: The global 21cm brightness temperature for the redshift range excluding the early stages of reionization. **Bottom:** The differences in brightness temperatures correspond to those in the ionization fractions, but have opposite signs. The typical differences are only $|\Delta T_b| \lesssim 0.7$ mK and are small compared to current observational sensitivities.

near the start and end of the EoR as expected. More accurate fits to simulation results can be obtained by combining both cases and using 5 rather than 3 ionization points. However, for parameter-space studies and constraining reionization histories from different observations, it is preferable to use a smaller number of free parameters to reduce degeneracies.

3.2. 21cm Brightness Temperature

The global 21cm brightness temperature (e.g. Madau et al. 1997) in units of mK is given by

$$\delta T_b \approx 28 x_{\text{HI}} \left(1 - \frac{T_\gamma}{T_s}\right) \left(\frac{\Omega_b h^2}{0.022}\right) \left[\left(\frac{0.15}{\Omega_m h^2} \frac{1+z}{10}\right)\right]^{1/2}, \quad (8)$$

where $x_{\text{HI}} = 1 - x_i$ is the neutral hydrogen fraction, T_γ is the radiation temperature, and T_s is the spin temperature. The standard approximation $T_s \gg T_\gamma$ is used, which is a valid assumption except in the early stages of reionization (e.g. Santos et al. 2008).

Figure 2 shows the evolution of the brightness temperature for the ranges $5.5 < z < 12$ and $x_{\text{HI}} \lesssim 0.8$. The analytical parametrizations are excellent matches to the simulation results as expected. The differences in the brightness temperatures correspond to those in the ionization fractions, but have opposite signs. The typical differences are only $|\Delta T_b| \lesssim 0.7$ mK and are small compared to current observational sensitivities.

Global 21cm experiments such as EDGES (Bowman et al. 2008), SCI-HI (Voytek et al. 2014), SARAS (Singh et al. 2017), and PRIZM (Peterson et al. in prep) that observe up to a frequency of 200 MHz will probe the reionization of hydrogen. To model and interpret their signals, they can use this analytical parameterization and explore the parameter space to put constraints on the redshift midpoint and duration, and possibly weaker bounds on the asymmetry.

3.3. Thomson Optical Depth

The Thomson optical depth integrated from redshift 0 to z is given as

$$\tau(z) = \sigma_T \int_0^z \bar{n}_e(z) \left| \frac{cdt}{dz} \right| dz, \quad (9)$$

where the volume-averaged free electron number density,

$$\bar{n}_e = x_{\text{HII}}\bar{n}_{\text{H}} + x_{\text{HeII}}\bar{n}_{\text{He}} + 2x_{\text{HeIII}}\bar{n}_{\text{He}} \quad (10)$$

is related to the mean number densities ($\bar{n}_{\text{H}}, \bar{n}_{\text{He}}$) and mass-weighted ionization fractions ($x_{\text{HII}}, x_{\text{HeII}}, x_{\text{HeIII}}$) for hydrogen and helium. HI and HeI are jointly ionized during the EoR (e.g. Trac & Cen 2007). While HeII reionization is also extended (e.g. McQuinn et al. 2009; La Plante et al. 2017), the simple approximation of an instantaneous transition at $z \approx 3$ is sufficiently accurate for calculating the optical depth.

Figure 3 shows that the analytical parametrizations accurately reproduce the integrated optical depth τ from the simulations with typical differences of $|\Delta\tau| \lesssim 0.001$ ($\lesssim 2\%$). The shape parametrizations using Δ_{z90} and A_{z90} produce very small differences of $|\Delta\tau| \lesssim 2 \times 10^{-4}$ because the differences in the ionization fraction Δx_i have both positive and negative values which average to nearly zero over the EoR redshift range. For integrated statistics that are linear in x_i , I recommend using the parameterizations Δ_{z90} and A_{z90} .

Planck will soon provide an update on their current constraint of $\tau = 0.058 \pm 0.012$ (Planck Collaboration et al. 2016a) from measurements of the CMB temperature and polarization angular power spectra (Planck Collaboration et al. 2016b). Since the location and amplitude of the reionization bump is precisely set by the redshift midpoint and optical depth, using an analytical parametrization that exactly matches a given z_{50} and accurately produces a desired τ is highly advantageous. The current tanh function in CAMB (Lewis 2008) can be replaced with this more accurate and flexible parametrization.

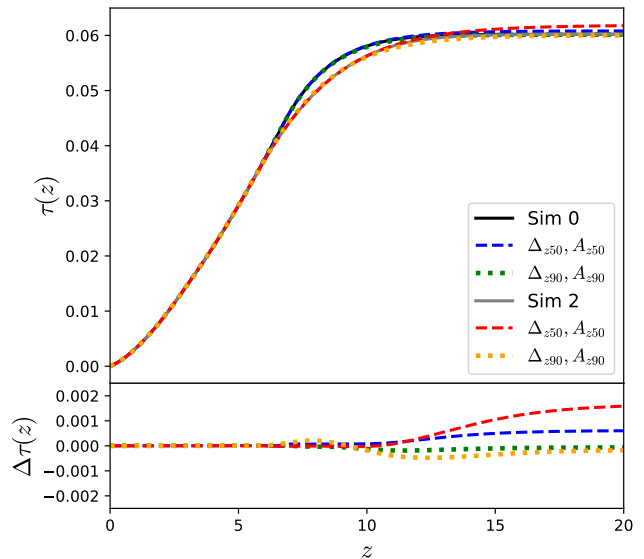


Figure 3. Top: The Thomson optical depth integrated up to redshift z . The SCORCH sims are designed to have fixed Thomson optical depth $\tau \approx 0.06$, consistent with recent CMB observations. **Bottom:** The differences in optical depths are smaller for parametrizations using Δ_{z90} and A_{z90} , which more effectively quantify the full extent of the EoR.

3.4. Patchy KSZ Effect

The KSZ temperature distortion (Sunyaev & Zel'dovich 1970) integrated along the direction $\hat{\mathbf{n}}$ is given by

$$\frac{\Delta T}{T}(\hat{\mathbf{n}}) = -\frac{\sigma_T}{c} \int n_e(\mathbf{v} \cdot \hat{\mathbf{n}}) e^{-\tau} \left| \frac{cdt}{dz} \right| dz, \quad (11)$$

where the electron number density n_e , peculiar velocity \mathbf{v} , and optical depth τ are all dependent on $\hat{\mathbf{n}}$ and z . In Battaglia et al. (2013), we choose to integrate over the redshift range $5.5 \leq z \leq 20$ for the patchy KSZ component since some models can have late end to reionization, like in Sim 2 here.

To quantify the impact of small differences in $x_i(z)$ on the patchy KSZ effect, I use a new and fast semi-numerical method of modeling reionization on large scales. In Holst et al. (in prep), we develop a novel approach that uses abundance matching to exactly satisfy a given $x_i(z)$. Density and velocity fields are constructed using 2nd-order Lagrangian perturbation theory (Scocimarro 1998) with 2048^3 particles in a periodic comoving box of side length $1 h^{-1} \text{Gpc}$. Full-sky HEALPix (Górski et al. 2005) maps with $N_{\text{side}} = 4096$ are then constructed by ray tracing through the simulated light cones.

Figure 4 shows the angular power spectrum $D_\ell \equiv \ell(\ell+1)C_\ell/(2\pi)$ in units of μK^2 . The overall amplitude is expected to increase with both the redshift midpoint and

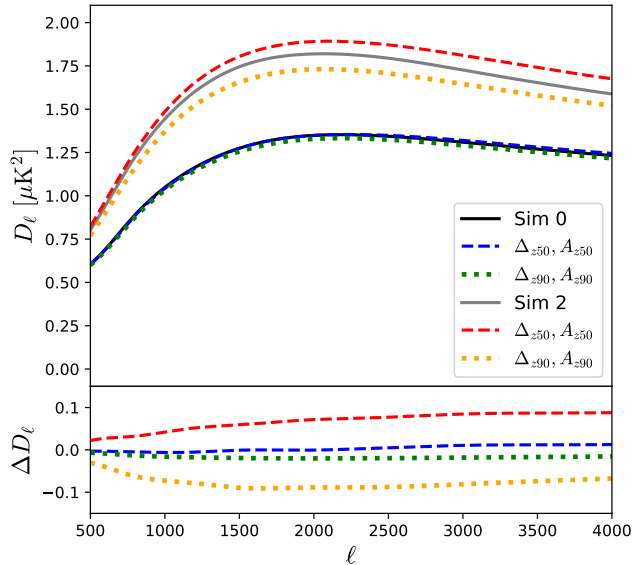


Figure 4. Top: The patchy KSZ angular power spectrum for temperature fluctuations integrated over the redshift range $5.5 < z < 20$. The overall amplitude increases for longer duration. **Bottom:** The differences in angular power have similar absolute values for both parametrizations, but there are larger differences for cases with larger $|\Delta x_i|$ and longer durations.

duration (e.g. Zahn et al. 2012; Battaglia et al. 2013). The shape parametrizations using Δ_{z50} and A_{z50} overpredict, while the those using Δ_{z90} and A_{z90} underpredict compared to the simulations. These trends correspond with the differences in the ionization fractions at higher redshifts $z > z_{50}$. There are also larger absolute differences for Sim 2 than Sim 0 because of the larger differences in $|\Delta x_i|$ and the longer duration. The maximum differences of $\Delta D_\ell \lesssim 0.1 \mu\text{K}^2$ ($\lesssim 5\%$) are expected to be atypical since Sim 2 has a rather long duration and late end to reionization at $z \lesssim 5.5$. In upcoming work,

I will explore the dependence of the patchy KSZ effect on the midpoint, duration, and asymmetry parameters.

Planck Collaboration et al. (2016a) combine their τ constraints with South Pole Telescope measurements of the KSZ angular power at $\ell = 3000$ (George et al. 2015), along with our KSZ theoretical models (Battaglia et al. 2013) to infer a duration $\Delta_{z\text{CMB}} \equiv z_{10} - z_{99} < 2.9$ (95% confidence interval). In Doussot et al. (2017), we find that the upper limit on the duration is in tension with our radiation-hydrodynamic simulations, all of which have longer durations. The current discrepancy most likely is due to assumptions made in the analyses, models, and simulations. Other contributing factors could be inconsistencies in parametrizing the reionization history and ambiguity in mass-weighted and volume-weighted ionization fractions.

4. CONCLUSIONS

I present an accurate parametrization of the reionization history in terms of the redshift midpoint, duration, and asymmetry. Lagrange interpolating functions are used to construct analytical curves which exactly fit corresponding ionization points. I recommend using the shape parameters Δ_{z90} and A_{z90} and caution against extreme choices (e.g. Δ_{z99}) since the start and end of the EoR are difficult to determine precisely. More accurate fits to simulation results can be obtained by using more ionization points, but a smaller number of free parameters is preferable for fitting observations. This accurate and flexible approach will allow parameter-space studies and self-consistent constraints on the reionization history from 21cm, CMB, and high-redshift galaxies and quasars.

I thank Nick Gnedin for the original motivation for this work. Thanks also go to Marcelo Alvarez, Nick Battaglia, Aristide Doussot, Ian Holst, and Sasha Kourov for helpful discussions. This work is supported by STScI grant HST-AR-15013.002-A.

REFERENCES

- Battaglia, N., Natarajan, A., Trac, H., Cen, R., & Loeb, A. 2013, *ApJ*, 776, 83, doi: [10.1088/0004-637X/776/2/83](https://doi.org/10.1088/0004-637X/776/2/83)
- Bond, J. R., & Efstathiou, G. 1987, *MNRAS*, 226, 655, doi: [10.1093/mnras/226.3.655](https://doi.org/10.1093/mnras/226.3.655)
- Bowman, J. D., Rogers, A. E. E., & Hewitt, J. N. 2008, *ApJ*, 676, 1, doi: [10.1086/528675](https://doi.org/10.1086/528675)
- Doussot, A., Aghanim, N., Ilić, S., & Langer, M. 2015, *A&A*, 580, L4, doi: [10.1051/0004-6361/201526543](https://doi.org/10.1051/0004-6361/201526543)
- Doussot, A., Trac, H., & Cen, R. 2017, *ArXiv e-prints*. <https://arxiv.org/abs/1712.04464>
- Furlanetto, S. R., Oh, S. P., & Briggs, F. H. 2006, *PhR*, 433, 181, doi: [10.1016/j.physrep.2006.08.002](https://doi.org/10.1016/j.physrep.2006.08.002)
- George, E. M., Reichardt, C. L., Aird, K. A., et al. 2015, *ApJ*, 799, 177, doi: [10.1088/0004-637X/799/2/177](https://doi.org/10.1088/0004-637X/799/2/177)
- Górski, K. M., Hivon, E., Banday, A. J., et al. 2005, *ApJ*, 622, 759, doi: [10.1086/427976](https://doi.org/10.1086/427976)
- La Plante, P., Trac, H., Croft, R., & Cen, R. 2017, *ApJ*, 841, 87, doi: [10.3847/1538-4357/aa7136](https://doi.org/10.3847/1538-4357/aa7136)
- Lewis, A. 2008, *PhRvD*, 78, 023002, doi: [10.1103/PhysRevD.78.023002](https://doi.org/10.1103/PhysRevD.78.023002)

- Loeb, A., & Furlanetto, S. R. 2013, The First Galaxies in the Universe
- Madau, P., Meiksin, A., & Rees, M. J. 1997, *ApJ*, 475, 429, doi: [10.1086/303549](https://doi.org/10.1086/303549)
- McQuinn, M., Lidz, A., Zaldarriaga, M., et al. 2009, *ApJ*, 694, 842, doi: [10.1088/0004-637X/694/2/842](https://doi.org/10.1088/0004-637X/694/2/842)
- Ostriker, J. P., & Vishniac, E. T. 1986, *ApJL*, 306, L51, doi: [10.1086/184704](https://doi.org/10.1086/184704)
- Planck Collaboration, Adam, R., Aghanim, N., et al. 2016a, *A&A*, 596, A108, doi: [10.1051/0004-6361/201628897](https://doi.org/10.1051/0004-6361/201628897)
- Planck Collaboration, Aghanim, N., Ashdown, M., et al. 2016b, *A&A*, 596, A107, doi: [10.1051/0004-6361/201628890](https://doi.org/10.1051/0004-6361/201628890)
- Richards, F. J. 1959, *Journal of Experimental Botany*, 10, 290, doi: [10.1093/jxb/10.2.290](https://doi.org/10.1093/jxb/10.2.290)
- Santos, M. G., Amblard, A., Pritchard, J., et al. 2008, *ApJ*, 689, 1, doi: [10.1086/592487](https://doi.org/10.1086/592487)
- Scoccimarro, R. 1998, *MNRAS*, 299, 1097, doi: [10.1046/j.1365-8711.1998.01845.x](https://doi.org/10.1046/j.1365-8711.1998.01845.x)
- Singh, S., Subrahmanyam, R., Udaya Shankar, N., et al. 2017, *ApJL*, 845, L12, doi: [10.3847/2041-8213/aa831b](https://doi.org/10.3847/2041-8213/aa831b)
- Sunyaev, R. A., & Zeldovich, Y. B. 1970, *Ap&SS*, 7, 3, doi: [10.1007/BF00653471](https://doi.org/10.1007/BF00653471)
- Trac, H., & Cen, R. 2007, *ApJ*, 671, 1, doi: [10.1086/522566](https://doi.org/10.1086/522566)
- Trac, H., Cen, R., & Mansfield, P. 2015, *ApJ*, 813, 54, doi: [10.1088/0004-637X/813/1/54](https://doi.org/10.1088/0004-637X/813/1/54)
- Trac, H., & Pen, U.-L. 2004, *New Astronomy*, 9, 443, doi: [10.1016/j.newast.2004.02.002](https://doi.org/10.1016/j.newast.2004.02.002)
- Voytek, T. C., Natarajan, A., Jáuregui García, J. M., Peterson, J. B., & López-Cruz, O. 2014, *ApJL*, 782, L9, doi: [10.1088/2041-8205/782/1/L9](https://doi.org/10.1088/2041-8205/782/1/L9)
- Zahn, O., Reichardt, C. L., Shaw, L., et al. 2012, *ApJ*, 756, 65, doi: [10.1088/0004-637X/756/1/65](https://doi.org/10.1088/0004-637X/756/1/65)
- Zaldarriaga, M. 1997, *PhRvD*, 55, 1822, doi: [10.1103/PhysRevD.55.1822](https://doi.org/10.1103/PhysRevD.55.1822)